Part I

Forward Model

The forward model as part of the MOBIIR scheme predicts the detector readings on the tissue boundary given a set of sources and the spatial distribution of optical properties. In Chapter 2 we introduce a forward model for light transport based on the time-independent **equation of radiative transfer**. We utilize a finite-difference discrete-ordinates method for discretizing the spatial and angular variables of the ERT. The resulting system of equations is solved by a successive overrelaxation method. The numerical error that is introduced due to the discretization of the ERT is evaluated in Chapter 3. The fluence on the boundary of tissue phantoms that contained **void regions** is compared to experimental results in Chapter 4.

Chapter 2

Photon Transport in Turbid Media

A main component of the MOBIIR scheme is the forward model for light propagation in tissue (see Subsection 1.2.1). The forward model calculates the detector predictions for a given set of spatially distributed optical parameters and source positions. The detector predictions are used in the inverse model for updating the optical parameters. The outcome of the reconstruction of the optical parameters largely depends on a sufficiently correct forward model for light transport. Until now, existing reconstruction techniques in OT cannot be applied to scattering media that include void-like areas. In this case the widely applied diffusion theory fails to describe the light propagation accurately enough and the reconstruction schemes provide erroneous results. Therefore, it is necessary to use a forward model based on the ERT, which correctly describes the migration of photons in void-like areas.

The mathematical description of the transport of particles such as neutrons, electrons, gas molecules, ions, and photons through a host medium is called transport theory. The goal of transport theory is to determine the distribution of these particles in the host medium, taking account of the motion of the particles and their interactions with the host

medium. Most of the applications of transport theory have developed almost independently of one another.

In the kinetic theory of gases Boltzmann developed the basic physics of transport processes of particles [Boltzmann1872] [Boltzmann64] over one century ago. The early development of the transport theory was stimulated by the radiant energy transfer in stellar or planetary atmospheres [Chandrasekhar60]. In 1905 the astrophysicist Schuster discussed the transmission of light through a foggy atmosphere taking light scattering effects besides emission and absorption into account [Schuster05]. Perhaps the most famous problem in transport theory is also known as the Milne problem [Milne21]. Near the center of a star photons are produced in the region of very high temperature. These photons escape through the stellar atmosphere and cross the boundary layer between the star and the surrounding vacuum. Mathematically, the problem is treated assuming a plane geometry with the source infinitely far from the boundary. Under these assumptions the angular distribution of the radiant energy and the resulting temperature distribution is calculated.

In the 1940s research was strongly focused on neutron transport theory because of the advent of the nuclear age [Lewis77]. Since then several analytical and numerical methods were elaborated that solve particle transport problems within a broad range of geometrical configurations and for heterogeneous media. These problems are typically encountered in nuclear reactors [Davison57] [Case67] [Duderstadt79] [Lewis84]. A concise historical overview is given by Zweifel [Zweifel78] [Zweifel97].

Currently, transport theory is applied to a variety of different fields in physics, e.g. in neutrino transport [Mezzacappa99], electron transport [Yamada89] [Abramo94], or in general for charged particles [Luo93]. Most recently transport theory was also applied to OT [Dorn98].

In this chapter, we describe the ERT as it applies to photon propagation in tissue.

Subsequently, methods for the numerical solution of this equation are discussed. Special emphasize is given to the derivation of the finite-difference discrete-ordinates method, which is used throughout the remainder of this work.

2.1 Equation of Radiative Transfer

The particle transport is mathematically described by the particle transport equation. It is a balance equation for the angular flux of particles. A derivation of this equation is given in [Duderstadt79]. The particle transport equation applied to photons is also called equation of radiative transfer (ERT) [Duderstadt79]. The ERT describes the transport of low energy photons through matter, such as human tissue, with absorbing and scattering properties. The three-dimensional time-independent ERT is given by:

$$\boldsymbol{\omega} \cdot \nabla \psi(\boldsymbol{r}, \boldsymbol{\omega}) + (\mu_a(\boldsymbol{r}) + \mu_s(\boldsymbol{r}))\psi(\boldsymbol{r}, \boldsymbol{\omega}) = S(\boldsymbol{r}, \boldsymbol{\omega}) + \mu_s(\boldsymbol{r}) \int_{4\pi} p(\boldsymbol{\omega}, \boldsymbol{\omega}')\psi(\boldsymbol{r}, \boldsymbol{\omega}')d\boldsymbol{\omega}'. \quad (2.1)$$

The fundamental quantity in radiative transport theory is the radiance $\psi(\boldsymbol{r}, \boldsymbol{\omega})$, with units of $\mathrm{Wcm}^{-2}\mathrm{sr}^{-1}$, at the spatial position $\boldsymbol{r}$ and unit direction $\boldsymbol{\omega}$. The spatial position and the direction of the radiance are defined by means of two coordinate systems [Duderstadt79]. A *laboratory coordinate system* describes the geometry of the medium in three-dimensional space. We have chosen *Cartesian* coordinates due to the medium geometry under consideration. Thus, each point of the medium is denoted by a vector $\boldsymbol{r} = \boldsymbol{r}(x, y, z)$. Furthermore, a *local coordinate system* describes the local scattering process of light along directions $\boldsymbol{\omega}$ at a particular point $\boldsymbol{r}$. The local coordinate system can be expressed in spherical coordinates with $\boldsymbol{\omega} = \boldsymbol{\omega}(\vartheta, \varphi)$. Both coordinate systems are shown in Figure 2.1. Furthermore, the integral of the radiance $\psi(\boldsymbol{r}, \boldsymbol{\omega})$ over all directions $\boldsymbol{\omega}$ at one point $\boldsymbol{r}$ yields the fluence $\phi(\boldsymbol{r})$

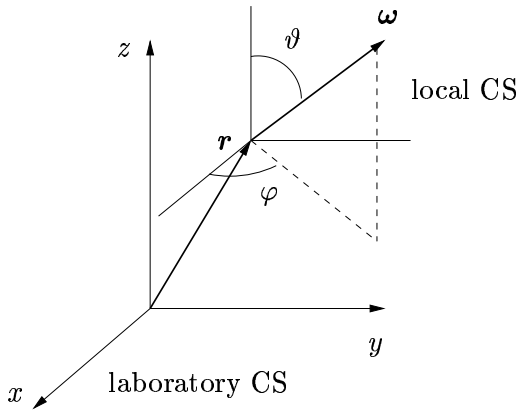

Figure 2.1: The laboratory coordinate system describes the global geometry of the scattering medium that contains all points $\boldsymbol{r}$. The local coordinate system describes the local scattering process into directions $\boldsymbol{\omega}$ at the point $\boldsymbol{r}$.

with units of Wcm^{-2}:

$$\phi(\boldsymbol{r}) = \int_{4\pi} \psi(\boldsymbol{r}, \boldsymbol{\omega}) d\boldsymbol{\omega}. \tag{2.2}$$

Other quantities besides the radiance ψ that are included in the ERT are the source term $S(\boldsymbol{r}, \boldsymbol{\omega})$ with the unit $\mathrm{Wcm}^{-3}\mathrm{sr}^{-1}$, the scattering coefficient, $\mu_s(\boldsymbol{r})$, the absorption coefficient, $\mu_a(\boldsymbol{r})$, both given in units of cm^{-1}, and the scattering phase function $p(\boldsymbol{\omega}, \boldsymbol{\omega}')$ with units of sr^{-1} [Patterson91].

The scattering phase function $p(\boldsymbol{\omega}, \boldsymbol{\omega}')$ in tissue optics is typically assumed to be spatially independent. It gives the probability that a single photon is deflected by an angle θ. The angle θ encloses the two directions formed by $\boldsymbol{\omega}$ and $\boldsymbol{\omega}'$ in the interval $\theta \in [0, \pi]$ with $\boldsymbol{\omega} \cdot \boldsymbol{\omega}' = \cos\theta$. A commonly applied scattering phase function in tissue optics is the Henyey-Greenstein function [Groenhuis83] [Prahl93]. This function was empirically introduced by Henyey and Greenstein for radiative transfer in galaxies [Henyey41] and is given as:

$$p(\cos\theta) = \frac{1 - g^2}{4\pi(1 + g^2 - 2g\cos\theta)^{3/2}}. \tag{2.3}$$

Other scattering phase functions [Chandrasekhar60] [Groenhuis83] besides the Henyey-Greenstein function have also been used in tissue optics, e.g. Mie scattering phase function [Mourant96] [Mourant98] or δ-Eddington phase function [Venugopalan98]. Furthermore, the phase function p is normalized with:

$$\int_{4\pi} p(\boldsymbol{\omega}, \boldsymbol{\omega}')d\boldsymbol{\omega}' = \int_{4\pi} p(\boldsymbol{\omega} \cdot \boldsymbol{\omega}')d\boldsymbol{\omega}' = \int_{4\pi} p(\cos\theta)d\boldsymbol{\omega}' = 1. \tag{2.4}$$

Assuming that the incoming direction $\boldsymbol{\omega}$ is parallel to the z-axis with $\vartheta = 0$ then the enclosed angle θ between $\boldsymbol{\omega}$ and the scattering direction $\boldsymbol{\omega}'$ is ϑ'. Thus, we have $\cos\theta = \cos\vartheta'$. Due to the azimuthal isotropy of the scattering process the phase function is independent of the angle φ' and we obtain

$$\int_0^{2\pi}\int_0^{\pi} p(\vartheta, \varphi, \vartheta', \varphi') \sin\vartheta' d\vartheta' d\varphi' = \int_0^{2\pi}\int_0^{\pi} p(\cos\vartheta') \sin\vartheta' d\vartheta' d\varphi' = 2\pi \int_0^{\pi} p(\cos\vartheta') \sin\vartheta' d\vartheta' = 1. \tag{2.5}$$

It is convenient to substitute the variable $\tau \in [-1, 1]$ for the factor $\cos\vartheta'$ and $\sin\vartheta' d\vartheta' = d\cos\vartheta' = d\tau$ within the integral. Therefore, the following identity holds for the integral:

$$2\pi \int_{-1}^{1} p(\tau)d\tau = 1. \tag{2.6}$$

Furthermore, the angular directions $\boldsymbol{\omega}$ of the radiance $\psi(\boldsymbol{r}, \boldsymbol{\omega})$ can also be expressed in Cartesian coordinates $\boldsymbol{\omega} = (\omega_x, \omega_y, \omega_z)$ with:

$$\begin{aligned} \omega_x &= \sin\vartheta\cos\varphi, \\ \omega_y &= \sin\vartheta\sin\varphi, \\ \omega_z &= \cos\vartheta, \end{aligned} \tag{2.7}$$

and consequently we obtain for the ERT with the scalar product $\boldsymbol{\omega} \cdot \nabla$

$$\sin\vartheta\cos\varphi\frac{\partial}{\partial x}\psi(\boldsymbol{r},\boldsymbol{\omega}) + \sin\vartheta\sin\varphi\frac{\partial}{\partial y}\psi(\boldsymbol{r},\boldsymbol{\omega}) + \cos\vartheta\frac{\partial}{\partial z}\psi(\boldsymbol{r},\boldsymbol{\omega}) + (\mu_a(\boldsymbol{r}) + \mu_s(\boldsymbol{r}))\psi(\boldsymbol{r},\boldsymbol{\omega}) = S(\boldsymbol{r},\boldsymbol{\omega}) + \mu_s(\boldsymbol{r})\int_{4\pi} p(\boldsymbol{\omega},\boldsymbol{\omega}')\psi(\boldsymbol{r},\boldsymbol{\omega}')d\boldsymbol{\omega}'. \tag{2.8}$$

The three-dimensional ERT (Equation 2.8) is an equation of three spatial variables (x, y, z) and two angular variables (φ, ϑ). Numerically finding solutions to this equation is in general a computationally very expensive task, both in terms of memory requirements and computational time. Therefore, the majority of works concerning the ERT deals with one-dimensional or two-dimensional problems, for which simplifying assumptions are introduced. In this work, we reduce the number of variables by imposing certain conditions to the medium geometry and source. First, assuming a medium with a translational invariance of the optical properties, μ_s and μ_a, and the source term S along z of the laboratory system yields a two-dimensional ERT that only depends on two spatial variables x, y and two angular variables φ, ϑ. Second, we further reduce the number of angular variables by only considering the scattering process within the $x - y$ plane by neglecting all *out-of-plane* directions with respect to the local coordinate system.

To derive the two-dimensional ERT we make the following assumptions with respect to the laboratory system. First, the geometry of the medium is independent of the coordinate z with $\mu_s = \mu_s(x, y)$ and $\mu_a = \mu_a(x, y)$. Second, the boundary condition of the medium is independent of z. Last, the source term S is independent of z with $S = S(x, y)$. We take the derivative of the ERT (Equation 2.8) with respect to z:

$$\frac{\partial}{\partial z}\left(\boldsymbol{\omega}\cdot\nabla\psi + (\mu_a(x,y) + \mu_s(x,y))\,\psi = S(x,y) + \mu_s(x,y)\int_{4\pi} p(\boldsymbol{\omega},\boldsymbol{\omega}')\psi d\boldsymbol{\omega}'\right). \tag{2.9}$$

We replace the derivative with $\breve{\psi} = \frac{\partial \psi}{\partial z}$ and we get:

$$\boldsymbol{\omega} \cdot \nabla \breve{\psi} + \psi \frac{\partial}{\partial z} \left(\mu_a(x,y) + \mu_s(x,y) \right) + \left(\mu_a(x,y) + \mu_s(x,y) \right) \breve{\psi} =$$
$$\frac{\partial}{\partial z} S(x,y) + \left(\frac{\partial}{\partial z} \mu_s(x,y) \right) \int_{4\pi} p(\boldsymbol{\omega}, \boldsymbol{\omega'}) \psi d\boldsymbol{\omega'} + \mu_s(x,y) \int_{4\pi} p(\boldsymbol{\omega}, \boldsymbol{\omega'}) \breve{\psi} d\boldsymbol{\omega'}. \tag{2.10}$$

The second term on the left-hand side and the first and second term on the right-hand side of Equation 2.10 vanish and we have

$$\boldsymbol{\omega} \cdot \nabla \breve{\psi} + \left(\mu_a(x,y) + \mu_s(x,y) \right) \breve{\psi} = \mu_s(x,y) \int_{4\pi} p(\boldsymbol{\omega}, \boldsymbol{\omega'}) \breve{\psi} d\boldsymbol{\omega'}. \tag{2.11}$$

The solution of Equation 2.11, which is Equation 2.1 having the source $S(x,y) = 0$, is $\breve{\psi} = 0$. We conclude that the radiance $\psi = \psi(x,y)$ is not a function of the spatial coordinate z. Therefore, we obtain the ERT for a two-dimensional plane:

$$\sin\vartheta \cos\varphi \frac{\partial}{\partial x} \psi(x,y,\boldsymbol{\omega}) + \sin\vartheta \sin\varphi \frac{\partial}{\partial y} \psi(x,y,\boldsymbol{\omega}) + \left(\mu_a(x,y) + \mu_s(x,y) \right) \psi(x,y,\boldsymbol{\omega}) =$$
$$S(x,y,\boldsymbol{\omega}) + \mu_s(x,y) \int_{4\pi} p(\boldsymbol{\omega}, \boldsymbol{\omega'}) \psi(x,y,\boldsymbol{\omega'}) d\boldsymbol{\omega'}. \tag{2.12}$$

This equation is, for example, also used in radiative heat transfer by Sakami *et al*, Wilson, Ramankutty, and Thynell [Sakami96] [Wilson96] [Ramankutty97] [Thynell98].

We further simplify Equation 2.12 with respect to the local coordinate system. We define two hemispheres S^1 and S^2 around a point $\boldsymbol{r} = (x, y, z_0)$ as depicted in Figure 2.2. The hemisphere S^1 sits on top of the $x-y$ plane and contains all directions $\hat{\boldsymbol{\omega}}$ that point towards $\boldsymbol{r}$. Hemisphere S^2 sits underneath the $x-y$ plane and contains all directions $\hat{\boldsymbol{\omega}}$ pointing towards $\boldsymbol{r}$. However, both hemispheres do not contain directions $\tilde{\boldsymbol{\omega}}$ that are within the $x-y$ plane. We assume that the radiance $\psi(\hat{\boldsymbol{\omega}})$ of out-of-plane directions $\hat{\boldsymbol{\omega}}$ negligibly contributes to the transport process within the $x-y$ plane due to the medium geometry along the z-axis. This assumption introduces a disparity of the radiance distribution with respect to Equation 2.12, that still needs to be qualitatively evaluated. We get as an

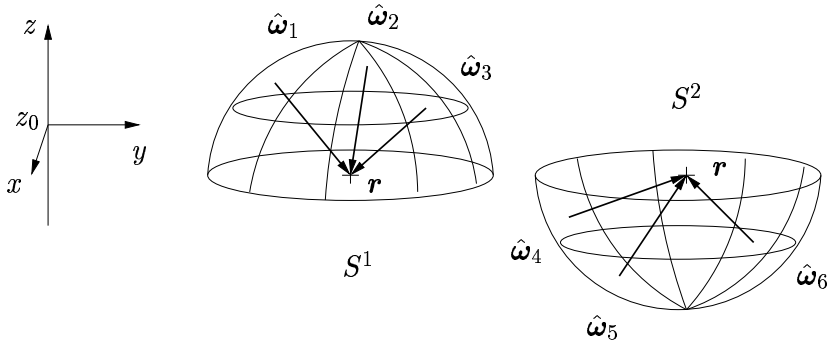

Figure 2.2: Hemispheres S^1 and S^2 around the point $\boldsymbol{r}$. S^1 is on top and S^2 is underneath of the $x-y$ plane at z_0. All directions $\hat{\boldsymbol{\omega}}$ point towards $\boldsymbol{r}$.

approximation:

$$\tilde{\boldsymbol{\omega}} \cdot \nabla\psi(\tilde{\boldsymbol{\omega}}) + (\mu_a + \mu_s)\psi(\tilde{\boldsymbol{\omega}}) = S(\tilde{\boldsymbol{\omega}}) + \mu_s \int_{2\pi} \tilde{p}(\tilde{\boldsymbol{\omega}}, \tilde{\boldsymbol{\omega}}')\psi(\tilde{\boldsymbol{\omega}}')d\tilde{\boldsymbol{\omega}}' \tag{2.13}$$

or

$$\cos\varphi\frac{\partial}{\partial x}\psi(x,y,\tilde{\boldsymbol{\omega}}) + \sin\varphi\frac{\partial}{\partial y}\psi(x,y,\tilde{\boldsymbol{\omega}}) + (\mu_a(x,y) + \mu_s(x,y))\psi(x,y,\tilde{\boldsymbol{\omega}}) = S(x,y,\tilde{\boldsymbol{\omega}}) + \mu_s(x,y)\int_{2\pi} \tilde{p}(\tilde{\boldsymbol{\omega}}, \tilde{\boldsymbol{\omega}}')\psi(x,y,\tilde{\boldsymbol{\omega}}')d\tilde{\boldsymbol{\omega}}'. \tag{2.14}$$

We replace all directions $\tilde{\boldsymbol{\omega}}$ with the angle φ and obtain with $\tilde{p}(\tilde{\boldsymbol{\omega}} \cdot \tilde{\boldsymbol{\omega}}') = \tilde{p}(\cos(\varphi - \varphi'))$:

$$\cos\varphi\frac{\partial}{\partial x}\psi(x,y,\varphi) + \sin\varphi\frac{\partial}{\partial y}\psi(x,y,\varphi) + (\mu_a(x,y) + \mu_s(x,y))\psi(x,y,\varphi) = S(x,y,\varphi) + \mu_s(x,y)\int_0^{2\pi} \tilde{p}(\cos(\varphi - \varphi'))\psi(x,y,\varphi')d\varphi'. \tag{2.15}$$

The scattering phase function $p(\cos\theta) = p(\cos(\varphi - \varphi'))$ (Equation 2.3) within the $x-y$ plane is normalized to unity to obtain energy conservation:

$$\tilde{p}(\cos(\varphi - \varphi')) := \frac{p(\cos(\varphi - \varphi'))}{\int_0^{2\pi} p(\cos(\varphi - \varphi'))d\varphi'}. \tag{2.16}$$

Johnson and Pitkäranta, Asadzadeh, Turek, Norton, Banoczi, Bal, Dorn, and Tamasan solve the two-dimensional ERT (Equation 2.13 - 2.15) in radiative heat transfer, neutron transport, and tissue optics by using only directions within the $x - y$ plane [Johnson83] [Asadzadeh86] [Asadzadeh89] [Turek93] [Norton97] [Dorn98] [Banoczi99] [Bal00a] [Bal00b] [Dorn00] [Tamasan02].

An error analysis of Equation 2.13 due to the negligence of out-of-plane directions $\hat{\boldsymbol{\omega}}$ does not exist in literature. One possible approach to evaluate the model error could be a direct comparison of solutions of Equation 2.13 to solutions of other light propagation models. For example, Bal compared solutions of Equation 2.13 to solutions of the diffusion equation for highly-scattering and void-like media [Bal01] [Bal02]. These comparisons show a match of transport-theory-based with diffusion-theory-based calculations on the boundary of homogeneous media, whereas a mismatch due to the failure of diffusion theory in void areas was found. However, even for homogeneous and highly-scattering media, where diffusion theory holds as an approximation to the ERT, a comparison of solutions to the ERT might be of questionable value. For example, in recent publications different groups have presented contradicting arguments concerning the inclusion of the absorption coefficient into the diffusion coefficient [Durduran97] [Aronson99] [Chen01]. Furthermore, the diffusion-boundary condition for tissue-like media makes use of a heuristically introduced factor that has to be determined experimentally and is not very reliable [Aronson95].

A better approach for validation is the direct comparison to experimental results as we are going to show in Chapter 4. The main criterion for a match of numerical and experimental results is that the forward model based on Equation 2.13 as part of the MOBIIR scheme predicts correctly the detector readings on the boundary of a tissue-like medium. These detector readings constitute numbers (in arbitrary units [a.u.]) that are proportional to the fluence ϕ (in units of Wcm^{-2}) on the boundary of the scattering medium. More-

over, the comparison of relative fluence data, due to unknown source strength and unknown coupling factors at the detector-tissue interface, is a standard procedure in OT [Pogue95] [Jiang96b] [Venugopalan98] [Boas01].

2.2 Numerical Methods to the Solution of the Equation of Radiative Transfer

Except for highly idealized problems [Case67] [Duderstadt79], solutions of the ERT are accomplished by numerical means, e.g. in [Stenholm91] [Turek93] [Kisselev94] [Turek95] [Chen98] [Folini99]. The choice of a given numerical technique depends on the approximations one uses to describe the properties of the medium and its geometrical configuration. Numerical solutions to the particle transport equation are obtained, for example, by using one of its three formulations: the integral, the surface-integral, or the integro-differential form [Lewis77] [Duderstadt79] [Sanchez82] [Lewis84]. The ERT as shown in Equation 2.1 and 2.13 is the integro-differential form. This form is widely used for the treatment of optically thick media, which we typically encounter in tissue optics. In the following work we will only focus on the numerical solution of this integro-differential form.

In general, numerical methods convert the integro-differential equation into a system of algebraic equations. The radiance $\psi(\boldsymbol{r}, \boldsymbol{\omega})$, which is a continuous function in space, is replaced by a finite set of $\mathcal{N}$ values. The transport equation is replaced by a set of approximate algebraic equations for each of these $\mathcal{N}$ values. These numerical techniques include, for example, the singular eigenfunction expansion method, the spherical harmonics method (P_N-method), and the discrete-ordinates method (S_N-method) [Sanchez82].

The similarity between the P_N-method and the S_N-method is that an approximation is used for eliminating the integral term in the ERT. The P_N-method expands the

the radiance in terms of eigenfunctions (e.g. spherical harmonics) of the integral operator. After truncation of this expansion a set of coupled differential equations for the expansion coefficients is obtained. On the other hand, the S_N-method uses a numerical quadrature in the angular variable to obtain an approximation of the integral term. The resulting set of coupled ordinary differential equations for the radiance in the directions specified by the quadrature formula is solved either by a finite-difference method or by the method of characteristics [Case67] [Carlson76] [Duderstadt79].

2.3 Finite-Difference Discrete-Ordinates Method

The S_N-method is employed with several finite-difference approximations [Carlson68] [Lathrop72]. Commonly applied finite-difference methods [Richtmyer67] are the diamond-differencing scheme [Alcouffe77], the weighted diamond-differencing scheme [Lathrop69] [Reed71b][Alcouffe93], the centered-differencing scheme [Davis67], the weighted central-differencing scheme [Madsen75], and the step function difference scheme.

The step function difference scheme or step method is applied in many fields, such as neutron transport theory [Carlson68] [Duderstadt79] [Lewis84], neutrino transport [Mezzacappa99], and in radiative transport in thermal plasma [Menart00]. The step method is also known as upwind scheme in the fields of fluid dynamics [Sewell88] [Fletcher90] and heat transfer [Zurigat90].

We use the upwind scheme in connection with the discrete-ordinates method to the ERT as a computationally efficient method for the calculation of the radiance. It has the advantage over other difference schemes that it supplies the necessary mathematical structure for the adjoint derivative calculation. The adjoint derivative calculation is central to the solution of the inverse problem and is the focus of Part II of this work.

2.3.1 Spatial and Angular Discretization

To solve the ERT (Equation 2.13 - 2.15) using an upwind-difference discrete-ordinates method the angular and spatial variables, $\tilde{\boldsymbol{\omega}}$ and $\boldsymbol{r}$, have to be discretized. First, the integral term

$$\mu_s \int_{2\pi} \tilde{p}(\tilde{\boldsymbol{\omega}}, \tilde{\boldsymbol{\omega}}')\psi(\boldsymbol{r}, \tilde{\boldsymbol{\omega}}')d\tilde{\boldsymbol{\omega}}' = \mu_s \int_0^{2\pi} \tilde{p}(\cos(\varphi - \varphi'))\psi(\boldsymbol{r}, \varphi')d\varphi' \tag{2.17}$$

in Equation 2.13 or 2.15 is replaced by a quadrature formula that uses a finite set of K angular directions $\tilde{\boldsymbol{\omega}}_{\mathrm{k}}$, represented by φ_{k}, with $\mathrm{k} \in [1, \mathrm{K}]$:

$$\mu_s \sum_{k'} a_{\mathrm{k}'} \left\{ \frac{\mathrm{K}}{2\pi} \int_{-\frac{\pi}{\mathrm{K}}}^{\frac{\pi}{\mathrm{K}}} \tilde{p}(\varphi_{\mathrm{k}} - \varphi_{\mathrm{k}'} + \beta)d\beta \right\} \psi(\boldsymbol{r}, \varphi_{\mathrm{k}'}) = \mu_s \sum_{k'} a_{\mathrm{k}'} \tilde{p}_{\mathrm{kk}'} \psi_{\mathrm{k}'}(\boldsymbol{r}). \tag{2.18}$$

The angular discretization yields a set of K coupled differential equations for the radiance $\psi(\boldsymbol{r}, \tilde{\boldsymbol{\omega}}_{\mathrm{k}}) = \psi(\boldsymbol{r}, \varphi_{\mathrm{k}}) = \psi_{\mathrm{k}}(\boldsymbol{r})$ in the directions $\tilde{\boldsymbol{\omega}}_{\mathrm{k}}$. The quadrature formula in Equation 2.18 is equivalent to the *extended trapezoidal rule* for numerical integration [Press92]. Hence, the parameter $a_{\mathrm{k}'}$ is a weighting factor with $a_{\mathrm{k}'} = \frac{2\pi}{\mathrm{K}}$, whereas the coefficient $\tilde{p}_{\mathrm{kk}'}$ constitutes the mean value of $\tilde{p}$ within the interval $\left[\varphi_{\mathrm{k}} - \varphi_{\mathrm{k}'} - \frac{\pi}{\mathrm{K}}, \varphi_{\mathrm{k}} - \varphi_{\mathrm{k}'} + \frac{\pi}{\mathrm{K}}\right]$. We show all coefficients $a_{\mathrm{k}'}\tilde{p}_{\mathrm{kk}'}$ for $\mathrm{K} = 16$ and $\mathrm{K} = 32$ ordinates for several anisotropy factors g in Appendix A.

Additionally, the spatial variable $\boldsymbol{r}$ needs to be discretized. The domain Ω is defined by a rectangular spatial mesh with I grid points on the x-coordinate and J grid points on the y-coordinate. The distance between adjacent grid points along the x-axis is Δx and along the y-axis is Δy. The radiance $\psi(\boldsymbol{r}, \varphi_{\mathrm{k}})$ at a grid point (i, j) with position $\boldsymbol{r} = (x_{\mathrm{i}}, y_{\mathrm{j}})$ and indices $\mathrm{i} \in [1, \mathrm{I}]$ and $\mathrm{j} \in [1, \mathrm{J}]$ for a particular direction $\tilde{\boldsymbol{\omega}}_{\mathrm{k}}$ with angle φ_{k} is represented by $\psi_{\mathrm{kij}} = \psi_{\mathrm{k}}(x_{\mathrm{i}}, y_{\mathrm{j}})$. The direction $\tilde{\boldsymbol{\omega}}_{\mathrm{k}}$ is expressed in Cartesian coordinates with $\xi_{\mathrm{k}} = \boldsymbol{e}_x \cdot \tilde{\boldsymbol{\omega}}_{\mathrm{k}} = \cos\varphi_{\mathrm{k}}$ and $\eta_{\mathrm{k}} = \boldsymbol{e}_y \cdot \tilde{\boldsymbol{\omega}}_{\mathrm{k}} = \sin\varphi_{\mathrm{k}}$.

Finally, the spatial derivatives have to be replaced with a finite-difference scheme. In this work we use an upwind-difference scheme. The upwind-difference formula depends

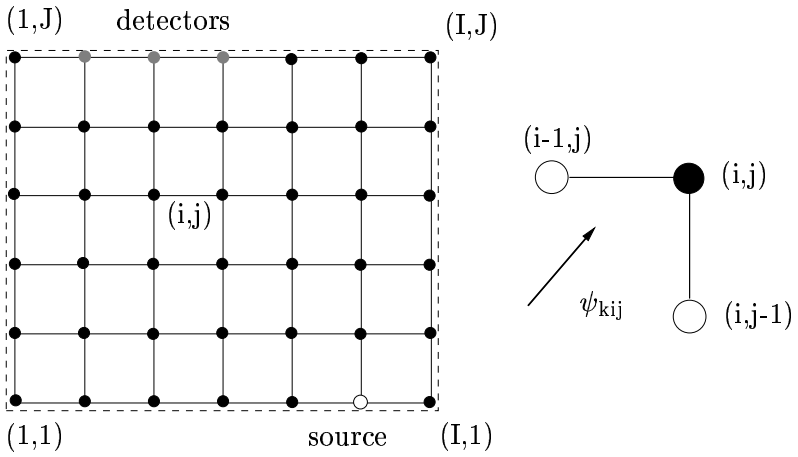

Figure 2.3: Finite-difference grid.

on the direction $\tilde{\boldsymbol{\omega}}_{\mathrm{k}}$ of the angular-dependent radiance ψ_{kij}. Thus, the set of all directions $\tilde{\boldsymbol{\omega}}_{\mathrm{k}}$ are subdivided into four quadrants and we get four different difference formulas for the radiance ψ_{kij}:

$$\left.\begin{aligned}
\xi_{\mathrm{k}} > 0\ ,\ \eta_{\mathrm{k}} > 0: &\quad \frac{\partial\psi}{\partial x} \approx \delta_x\psi_{\mathrm{kij}} = \frac{\psi_{\mathrm{ij}} - \psi_{\mathrm{i-1j}}}{\Delta x}\ ,\ \frac{\partial\psi}{\partial y} \approx \delta_y\psi_{\mathrm{kij}} = \frac{\psi_{\mathrm{ij}} - \psi_{\mathrm{ij-1}}}{\Delta y} \\
\xi_{\mathrm{k}} < 0\ ,\ \eta_{\mathrm{k}} > 0: &\quad \frac{\partial\psi}{\partial x} \approx \delta_x\psi_{\mathrm{kij}} = \frac{\psi_{\mathrm{i+1j}} - \psi_{\mathrm{ij}}}{\Delta x}\ ,\ \frac{\partial\psi}{\partial y} \approx \delta_y\psi_{\mathrm{kij}} = \frac{\psi_{\mathrm{ij}} - \psi_{\mathrm{ij-1}}}{\Delta y} \\
\xi_{\mathrm{k}} > 0\ ,\ \eta_{\mathrm{k}} < 0: &\quad \frac{\partial\psi}{\partial x} \approx \delta_x\psi_{\mathrm{kij}} = \frac{\psi_{\mathrm{ij}} - \psi_{\mathrm{i-1j}}}{\Delta x}\ ,\ \frac{\partial\psi}{\partial y} \approx \delta_y\psi_{\mathrm{kij}} = \frac{\psi_{\mathrm{ij+1}} - \psi_{\mathrm{ij}}}{\Delta y} \\
\xi_{\mathrm{k}} < 0\ ,\ \eta_{\mathrm{k}} < 0: &\quad \frac{\partial\psi}{\partial x} \approx \delta_x\psi_{\mathrm{kij}} = \frac{\psi_{\mathrm{i+1j}} - \psi_{\mathrm{ij}}}{\Delta x}\ ,\ \frac{\partial\psi}{\partial y} \approx \delta_y\psi_{\mathrm{kij}} = \frac{\psi_{\mathrm{ij+1}} - \psi_{\mathrm{ij}}}{\Delta y}
\end{aligned}\right\} \tag{2.19}$$

The ERT with the external and internal source term on the right-hand side, can now be written as:

$$\xi_{\mathrm{k}}\delta_x\psi_{\mathrm{kij}} + \eta_{\mathrm{k}}\delta_y\psi_{\mathrm{kij}} + ([\mu_a]_{\mathrm{ij}} + [\mu_s]_{\mathrm{ij}})\psi_{\mathrm{kij}} = S_{\mathrm{kij}} + [\mu_s]_{\mathrm{ij}} \sum_{\mathrm{k'}} a_{\mathrm{k'}}\tilde{p}_{\mathrm{kk'}}\psi_{\mathrm{k'ij}} \tag{2.20}$$

and we get for example for the ordinates $\xi_{\mathrm{k}} > 0\ ,\ \eta_{\mathrm{k}} > 0$:

$$\xi_{\mathrm{k}}\frac{\psi_{\mathrm{kij}} - \psi_{\mathrm{ki-1j}}}{\Delta x} + \eta_{\mathrm{k}}\frac{\psi_{\mathrm{kij}} - \psi_{\mathrm{kij-1}}}{\Delta y} + ([\mu_s]_{\mathrm{ij}} + [\mu_a]_{\mathrm{ij}})\psi_{\mathrm{kij}} = S_{\mathrm{kij}} + [\mu_s]_{\mathrm{ij}} \sum_{\mathrm{k'}} a_{\mathrm{k'}}\tilde{p}_{\mathrm{kk'}}\psi_{\mathrm{k'ij}}. \tag{2.21}$$

Recasting the left-hand side of Equation 2.20 as a single operator acting upon ψ_{kij} we get

$$\{\xi_{\mathrm{k}}\delta_x + \eta_{\mathrm{k}}\delta_y + ([\mu_a]_{\mathrm{ij}} + [\mu_s]_{\mathrm{ij}})\}\psi_{\mathrm{kij}} = S_{\mathrm{kij}} + [\mu_s]_{\mathrm{ij}} \sum_{\mathrm{k}'} a_{\mathrm{k}'}\tilde{p}_{\mathrm{kk}'}\psi_{\mathrm{k}'\mathrm{ij}} \tag{2.22}$$

from which it is apparent that the system of equations corresponding to all K directions and I × J grid points can be written as a single matrix equation

$$\boldsymbol{A}\boldsymbol{\psi} = \boldsymbol{b}. \tag{2.23}$$

2.3.2 Successive Overrelaxation Method

The resulting system of equations is solved for the radiance vector $\boldsymbol{\psi}$ by a *Gauss-Seidel* method [Ames77]. Accordingly, we split the matrix $\boldsymbol{A}$ into a diagonal part $\boldsymbol{D}$, an upper triangular part $\boldsymbol{U}$, and a lower triangular part $\boldsymbol{L}$, with $\boldsymbol{A} = \boldsymbol{L} + \boldsymbol{D} + \boldsymbol{U}$. The original matrix equation (Equation 2.23) can now be written as

$$(\boldsymbol{L} + \boldsymbol{D} + \boldsymbol{U})\,\boldsymbol{\psi} = \boldsymbol{b}$$

or

$$(\boldsymbol{L} + \boldsymbol{D})\,\boldsymbol{\psi} = -\boldsymbol{U}\boldsymbol{\psi} + \boldsymbol{b}. \tag{2.24}$$

The iterative form with the iteration matrix $(\boldsymbol{L} + \boldsymbol{D})$ on the left-hand side is expressed as

$$(\boldsymbol{L} + \boldsymbol{D})\,\boldsymbol{\psi}^{\mathrm{z}+1} = -\boldsymbol{U}\boldsymbol{\psi}^{\mathrm{z}} + \boldsymbol{b}. \tag{2.25}$$

In order to break up the matrix $\boldsymbol{A}$ into $\boldsymbol{L} + D + U$ and also have $\boldsymbol{U} = 0$ we re-order the radiance vector $\boldsymbol{\psi}$ for all ordinates in the following way:

$$\left.\begin{aligned}
\xi_{\mathrm{k}} > 0\ ,\ \eta_{\mathrm{k}} > 0: &\quad \boldsymbol{\psi} = (\psi_{\mathrm{k11}}, \psi_{\mathrm{k12}}, ..., \psi_{\mathrm{k21}}, \psi_{\mathrm{k22}}, ..., \psi_{\mathrm{kij}}, ..., \psi_{\mathrm{kIJ-1}}, \psi_{\mathrm{kIJ}}) \\
\xi_{\mathrm{k}} < 0\ ,\ \eta_{\mathrm{k}} > 0: &\quad \boldsymbol{\psi} = (\psi_{\mathrm{kI1}}, \psi_{\mathrm{kI-11}}, ..., \psi_{\mathrm{kI2}}, \psi_{\mathrm{kI-12}}, ..., \psi_{\mathrm{kij}}, ..., \psi_{\mathrm{k2J}}, \psi_{\mathrm{k1J}}) \\
\xi_{\mathrm{k}} > 0\ ,\ \eta_{\mathrm{k}} < 0: &\quad \boldsymbol{\psi} = (\psi_{\mathrm{k1J}}, \psi_{\mathrm{k1J-1}}, ..., \psi_{\mathrm{k2J}}, \psi_{\mathrm{k2J-1}}, ..., \psi_{\mathrm{kij}}, ..., \psi_{\mathrm{kI2}}, \psi_{\mathrm{kI1}}) \\
\xi_{\mathrm{k}} < 0\ ,\ \eta_{\mathrm{k}} < 0: &\quad \boldsymbol{\psi} = (\psi_{\mathrm{kIJ}}, \psi_{\mathrm{kIJ-1}}, ..., \psi_{\mathrm{kI-1J}}, \psi_{\mathrm{kI-1J-1}}, ..., \psi_{\mathrm{kij}}, ..., \psi_{\mathrm{k12}}, \psi_{\mathrm{k11}})\,.
\end{aligned}\right\} \tag{2.26}$$

Thus, we get for example for $\xi_k > 0$, $\eta_k > 0$:

$$\underbrace{\left\{\frac{\xi_k}{\Delta x}+\frac{\eta_k}{\Delta y}+([\mu_a]_{ij}+[\mu_s]_{ij})\right\}\psi_{kij}^{z+1}}_{\text{diagonal matrix } \boldsymbol{D}} \underbrace{-\frac{\xi_k}{\Delta x}\psi_{ki-1j}^{z+1}-\frac{\eta_k}{\Delta y}\psi_{kij-1}^{z+1}}_{\text{lower matrix } \boldsymbol{L}} = \underbrace{S_{kij}+[\mu_s]_{ij}\sum_{k'}a_{k'}\tilde{p}_{kk'}\psi_{k'ij}^{z}}_{\boldsymbol{b}}. \tag{2.27}$$

As we can see, the upper matrix $\boldsymbol{U}$ vanishes and we obtain the iterative equation:

$$(\boldsymbol{L}+\boldsymbol{D})\,\boldsymbol{\psi}^{z+1}=\boldsymbol{b}, \tag{2.28}$$

where $\boldsymbol{b}$, as a function of $\psi_{k'ij}^{z}$, is updated after each iteration step. We solve this equation for ψ_{kij}^{z+1} explicitly:

$$\psi_{kij}^{z+1}=\frac{S_{kij}+[\mu_s]_{ij}\sum_{k'}a_{k'}\tilde{p}_{kk'}\psi_{k'ij}^{z}+\frac{\xi_k}{\Delta x}\psi_{ki-1j}^{z+1}+\frac{\eta_k}{\Delta y}\psi_{kij-1}^{z+1}}{\frac{\xi_k}{\Delta x}+\frac{\eta_k}{\Delta y}+([\mu_a]_{ij}+[\mu_s]_{ij})}, \tag{2.29}$$

because all ψ_{ki-1j}^{z+1} and ψ_{kij-1}^{z+1} on the right-hand side of Equation 2.29 were already calculated at the current iteration step $(z+1)$. This is a result of the particular vector ordering as shown in 2.26. The iteration process is stopped when the relative error norm, which is used in most transport codes [Reed71a],

$$\frac{|\psi_{kij}^{z+1}-\psi_{kij}^{z}|}{\psi_{kij}^{z}}<\zeta \tag{2.30}$$

of all boundary grid points (i,j) with ordinate index k is less than a predefined value ζ (typically 10^{-3} to 10^{-5}).

A significant improvement in convergence speed is achieved by a slight modification to the Gauss-Seidel method. The *successive overrelaxation* method (SOR) uses a relaxation parameter ρ with $1 \le \rho \le 2$ in order to correct the solution ψ_{kij}^{z+1} of the Gauss-Seidel-iteration, now denoted as $\overline{\psi_{kij}^{z+1}}$. The accepted new value ψ_{kij}^{z+1} of the SOR is extrapolated from the Gauss-Seidel value $\overline{\psi_{kij}^{z+1}}$ and the previous accepted value ψ_{kij}^{z} of the SOR using

$$\psi_{kij}^{z+1}=(1-\rho)\psi_{kij}^{z}+\rho\overline{\psi_{kij}^{z+1}}. \tag{2.31}$$

The parameter ρ is empirically chosen. We found that the best value is $\rho = 1.0 - 1.1$ for isotropic scattering and $\rho = 1.5 - 1.9$ for anisotropic scattering.

2.3.3 Boundary Conditions

The boundary grid points ψ_{kij} are modified between each successive iteration step according to the boundary condition. Because of the refractive index mismatch at the air-medium interface (refractive index of the medium is depicted by n_m with $n_m > n_0 = 1$), the incident radiance ψ_i is partly reflected on the boundary and only a fraction of that light, ψ_t', escapes the medium [Ishimaru89]. The internally reflected light, ψ_r, contributes further to the photon propagation inside the medium (see Figure 2.4).

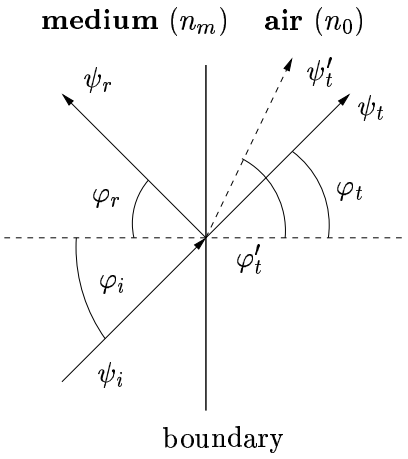

Figure 2.4: Boundary conditions at a grid point (i,j). The incident radiance ψ_i is partly reflected due to the refractive index mismatch at the air-tissue interface.

The angle φ_t', which pertains to a radiance ψ_t' escaping the medium, is determined by *Snell*'s law

$$n_m \sin \varphi_i = n_0 \sin \varphi_t' \tag{2.32}$$

given the angle φ_i of the radiance, which hits the boundary inside the medium. At this

point we make an approximation because one often has only a limited discrete set of φ_{k} (e.g. $\mathrm{K} = 8, 16$). We do not change the direction and define the angles

$$\varphi_t := \varphi_i \tag{2.33}$$

instead of using Equation 2.32 of calculating φ_t'. For example, an incoming radiance at the boundary with $\varphi_i = 25^{\mathrm{o}}$ has an outgoing radiance with $\varphi_t' = 39.3^{\mathrm{o}}$ according to Snell's law ($n_m = 1.5$). However, the outgoing radiance with φ_t' pertains to the same discrete ordinate $\boldsymbol{\omega}_{\mathrm{k}}$, depicted by φ_{k}, as the incoming radiance with φ_i when $\mathrm{K} = 16$. Hence, both angles, φ_t and φ_t', cannot be distinguished within the numerical scheme due to the angular discretization $\frac{360^{\mathrm{o}}}{\mathrm{K}} = 22.5^{\mathrm{o}} > \varphi_t' - \varphi_i$. Furthermore, we take total reflection into account for large angles φ_i.

Using *Fresnel*'s formula, the transmissivity T and reflectivity R are calculated at the boundary grid points (i, j) for each ordinate index k. The reflectivity R and transmissivity T are defined as:

$$R = \frac{1}{2}\left(\frac{\sin^2(\varphi_t' - \varphi_i)}{\sin^2(\varphi_t' + \varphi_i)} + \frac{\tan^2(\varphi_t' - \varphi_i)}{\tan^2(\varphi_t' + \varphi_i)}\right) \tag{2.34}$$

and

$$T = 1 - R. \tag{2.35}$$

The angle of the reflected radiance ψ_r on the boundary inside the medium is given by $\varphi_r = -\varphi_i$. Finally, the transmitted and reflected radiance are calculated with:

$$\psi_t = T \cdot \psi_i \tag{2.36}$$

$$\psi_r = R \cdot \psi_i. \tag{2.37}$$

The reflected radiance ψ_r is further used within the z-th iteration process. It modifies the old value of the radiance $\psi^{\mathrm{z}}_{\mathrm{kij}}$ at the boundary grid point (i,j) and ordinate index k. The

transmitted radiance ψ_t modifies the outgoing radiance $\psi^{\mathrm{Z}}_{\mathrm{kij}}$ of the final iteration step Z at a given boundary grid point (i, j). The fluence ϕ_{ij} on that particular boundary grid point (i, j) is determined by only using ordinates $\tilde{\boldsymbol{\omega}}_{\mathrm{k}}$ that enter the detector aperture AP:

$$\phi_{\mathrm{ij}} = \sum_{\mathrm{k}\in\mathrm{AP}} a_{\mathrm{k}} \psi_{\mathrm{kij}}. \tag{2.38}$$

Here, the parameter a_{k} is a weighting factor given by the extended trapezoidal rule [Press92].

2.4 Discussion

We have employed a finite-difference discrete-ordinates method to discretize the ERT. An upwind-difference scheme was used for the spatial discretization, and discrete ordinates were used for the angular discretization of the radiance $\psi(\boldsymbol{r}, \tilde{\boldsymbol{\omega}})$. The resulting system of difference equations was solved for the radiance by a SOR method.

The main focus of the choice of a forward model for light transport within a MOBIIR scheme was the convergence speed towards the solution besides the numerical accuracy of the solution, which will be discussed in the next Chapter 3. We found that the processing time depends on the number I × J of grid points, number K of ordinates, the overrelaxation parameter ρ, and the optical parameters μ_s, μ_a, and g.

Typical numerical examples, that can be found throughout this work, have approximately 61 × 61 or 81 × 81 grid points and 16 discrete ordinates. Assuming optical parameters of $\mu_{\mathrm{s}} = 11.6$ cm^{-1}, $\mu_{\mathrm{a}} = 0.35$ cm^{-1}, and $g = 0$, the SOR method needed 280-300 iteration steps for $\zeta = 10^{-5}$. That amounts in 20-60 seconds calculation time by using a PENTIUM III XEON® processor. Furthermore, we found that the processing time decreases linearly when μ_a is increased, or μ_s is decreased. However, the calculation time is unchanged for examples where μ_s and g were altered simultaneously while $\mu_s' = (1 - g)\mu_s$ was held constant.